2018 SCEC Annual Report

SDSU BBP Module Extension: Temporal-Spatial Ground Motion Correlation

Report for SCEC Award 18146

PI: Dr. Kim B. Olsen

Institution: Department of Geological Sciences, San Diego State University, San Diego, CA 92182-1020

Publications and Reports:

Wang, N., R. Takedatsu, K.B. Olsen, and S.M. Day (2018). Implementing Inter-Period Correlations into the SDSD Broadband Ground Motion Method, *Seism. Res. Lett.* **89**, 2B, 934.

Wang, N., R. Takedatsu, K.B. Olsen, and S.M. Day (2018). Implementing Inter-Period Correlations into the SDSD Broadband Ground Motion Method, *SCEC Annual Mtg,* Palm Springs, Sept 8-12, Poster #010.

Summary
Ground motion simulations can be viable alternatives to empirical relations for seismic hazard analysis when data are sparse. However, in many cases, simulated ground motion time series, in particular those originating from stochastic methods, lack inter-frequency correlation revealed in recorded seismic data, which has implications for seismic risk. We develop a post-processing method to rectify simulation techniques that otherwise produce synthetic time histories deficient in inter-frequency correlation structure.

Fourier Amplitude Spectrum (FAS) and Effective Amplitude Spectrum (EAS)
The Effective Amplitude Spectrum (EAS), defined by Kottke *et al.* (2018) as

$$EAS(f) = \sqrt{\frac{1}{2}[FAS_{HC1}^2(f) + FAS_{HC2}^2(f)]}\,, \qquad \text{Eq. 1}$$

is used as the intensity measure in our study. In Eq. 1, FAS_{HC1} and FAS_{HC2} are the FAS of the two as-recorded horizontal components of a three component acceleration time series, and f is the frequency in Hertz. The EAS is independent of the recording instrument's orientation. The EAS is smoothed using the $\log_{10}$-scale Konno and Ohmachi (1998) smoothing window selected by Kottke *et al.* (2018):

$$W(f) = \left(\frac{\sin\left(b\log(f/f_c)\right)}{b\log(f/f_c)}\right)^4, \qquad \text{Eq. 2}$$

$$b = \frac{2\pi}{b_w}, \qquad \text{Eq. 3}$$

where W is the weight defined at frequency f for a window with center frequency f_c, b is the window parameter, and $b_w = \frac{1}{30}$ is the bandwidth of the smoothing window in $\log_{10}$ units. For more details on the smoothing technique, the reader is referred to Kottke *et al.* (2018).

Inter-Frequency Correlations of Within-Event Residuals
We follow the notation defined by Al Atik *et al.* (2010):

$$y_{es} = \mu_{es} + \delta B_e + \delta W_{es}\,, \qquad \text{Eq. 4}$$

where y_{es} is the natural logarithm of the ground-motion intensity measure observed at station s during earthquake e, and μ_{es} is the mean prediction of the natural logarithm of the intensity measure. δB_e is the between-event residual (or inter-event residual), representing the average shift of the observed ground motion for an individual earthquake e from the population mean prediction. δW_{es} is the within-event residual (or intra-event residual), depicting the misfit between an individual observation at station s from the earthquake-specific mean prediction. The source effect average (over all azimuths) is described by the between-event residual that reflects the influence of factors such as stress drop and variation of slip in time and space that cannot be captured by the inclusion of magnitude, faulting style, and source depth in the mean prediction. Azimuthal variations in source, path, and site effects are described by the within-event residual that reflects the influence of factors such as crustal heterogeneity, deeper geological structure, and near-surface layering that cannot be captured by a simple distance metric and a site-classification based on the average shear-wave velocity (Al Atik, et al., 2010). These residuals are normally distributed with zero mean and are uncorrelated with each other.

In this study, we target the EAS within-event residual through epsilon (ε),

$$\varepsilon(f) = \frac{\delta W_{es}(f)}{\varphi(f)} = \frac{\ln EAS_{es}(f) - \mu_{\ln EAS_{es}}(f) - \delta B_e}{\varphi(f)}, \qquad \text{Eq. 5}$$

the within-event residual normalized by its standard deviation φ. The value of the within-event residual of EAS depends on frequency f. By the normalization, epsilon is standard normally distributed with zero mean and unit standard deviation.

For a given set of observations, the values of ε at neighboring frequencies (f) are probabilistically correlated. If a ground motion intensity measure is stronger than average at a certain frequency, then it tends to also be stronger at nearby frequencies; however, the ε values are weakly correlated if the frequency pair are widely-separated (Bayless and Abrahamson, 2018b). The correlation coefficient of ε at two frequencies f_1 and f_2 can be estimated by the maximum likelihood estimator (Kutner *et al*., 2004) using the Pearson product-moment correlation coefficient (Fisher, 1958),

$$\rho_{\varepsilon(f_1)\varepsilon(f_2)} = \frac{\sum_{i=1}^{n}\left(\varepsilon_i(f_1) - \overline{\varepsilon(f_1)}\right)\left(\varepsilon_i(f_2) - \overline{\varepsilon(f_2)}\right)}{\sqrt{\sum_{i=1}^{n}\left(\varepsilon_i(f_1) - \overline{\varepsilon(f_1)}\right)^2}\sqrt{\sum_{i=1}^{n}\left(\varepsilon_i(f_2) - \overline{\varepsilon(f_2)}\right)^2}}, \qquad \text{Eq. 6}$$

in which n is the number of observations, $\varepsilon_i(f_1)$ and $\varepsilon_i(f_2)$ represent the ith observation of ε at frequencies f_1 and f_2, respectively, $\overline{\varepsilon(f_1)}$ and $\overline{\varepsilon(f_2)}$ are their sample means, and the expectations of $\overline{\varepsilon(f_1)}$ and $\overline{\varepsilon(f_2)}$ are both zero. This correlation is important when simulated time histories are used for seismic risk analysis because variability in the dynamic structural response will be underestimated if the inter-frequency correlation in simulated ground motions is unrealistically low (Bayless and Abrahamson, 2018b).

Bayless and Abrahamson (2018a) generated an empirical estimate of ρ for the EAS within-event residual using the NGA-West2 database (regression from shallow crustal earthquakes, with M>3) at frequencies from 0.1 Hz to 24 Hz. The epsilon at each frequency was calculated from the individual EAS values and the earthquake-specific smoothed EAS median model for each recorded event at each station. Then, $\rho_{\varepsilon(f_1)\varepsilon(f_2)}$ was calculated for each pair of frequencies, f_1 and f_2 . Figure 1 shows the empirical correlation coefficients.

Inclusion of Inter-frequency Correlation in FAS

The procedure to generate a new ground motion time series with realistic inter-frequency correlations is as follows:

(1) take the Fourier transform of the two horizontal components of the synthetic ground motion time series. For each component, let the number of frequency points be n, the Fourier amplitude and phase at the ith frequency be $Amp_{ori}(i)$ and $Ph_{ori}(i)$, respectively;
(2) for each of the horizontal components, sample a normally distributed vector-valued random variable R with zero mean, a constant standard deviation, σ, and size n;
(3) express the empirical covariance $\rho_{\varepsilon(f_1)\varepsilon(f_2)}$ from Eq. 6 in matrix form Σ (n by n, real, symmetric, and positive definite), and apply the Cholesky decomposition of Σ as

$$\Sigma = \mathrm{K}\mathrm{K}^{\mathrm{T}}, \qquad \text{Eq. 7}$$

where K is a n by n lower triangular matrix (Seydel, 2012);
(4) left multiply random variable R in (3) by K as

$$S = KR\ , \qquad \text{Eq. 8}$$

to generate a normal random variable S with zero mean and covariance equal to $\sigma^2\mathrm{K}\mathrm{K}^{\mathrm{T}} = \sigma^2\Sigma$ (Seber and Lee, 2012);
(5) multiply the exponential of S with Amp_{ori} to compute the Fourier amplitude of the new ground motion synthetics, Amp_{new}, as

$$Amp_{new}(i) = Amp_{ori}(i)\exp S_i\ ; \qquad \text{Eq. 9}$$

(6) calculate the new ground-motion time series by applying the inverse Fourier transform to the spectrum obtained in (5).

The method can be applied as the last step to simulate the ground-motion using the SDSU SCEC BBP module, and thus classified as post-processing. It retains the mean of the Fourier amplitude for the updated ground-motion synthetics, since the mean of $\exp S_i$ in step (5) equals 1. Taking the natural logarithm of the equation in step (5) we get

$$\ln Amp_{new}(i) = \ln Amp_{ori}(i) + S_i\ . \qquad \text{Eq. 10}$$

We tested our method by calculating the within-event residual for the Loma Prieta event on the SCEC BBP. It is important to emphasize that the results generated using different source realizations from the kinematic source generator module by Graves and Pitarka (2015) for that validation event should be treated as different events, rather than multiple realizations of the same event. The reason for this is that the source realizations have variations in hypocenter locations and slip distributions that are represented by the between-event residual. Then, for each event, we generate 10 realizations at all the stations from each of the 50 'events' by changing the seed number in the random number generator for the scatterograms. For each set of 10 realizations, the mean of the 10 simulations and the within-event residual at each station are computed. The within-event residual at all stations and all realizations of the 'events' are pooled together by their corresponding frequency. Note, that if the total number of stations is m, then at each frequency f the epsilon of the within-event residual $\varepsilon(f)$ has a size equal to $10\ realizations\ by\ 50\ 'events'\ by\ m = 500\ m$.

Figure 1 shows that the resulting inter-frequency correlation coefficients obtained by our method for the Loma Prieta validation event compare very well with the empirical result, as intended. From Figure 2 it is clear that the addition of correlation to the synthetic time histories results in insignificant changes in the bias. The method generates correlated synthetic time series that are very similar to the original results from current SDSU BBP Module. Figure 3 shows one component of synthetic time histories (velocity and acceleration) and FAS, respectively, at station 8001-CLS for the Loma Prieta validation event before and after implementing the inter-frequency correlations. The method can be used as a post-processing step to incorporate the correlation into

an already established and validated ground motion generator. Finally, Figure 4 shows that our method also works well to incorporate realistic inter-frequency correlation into PSA.

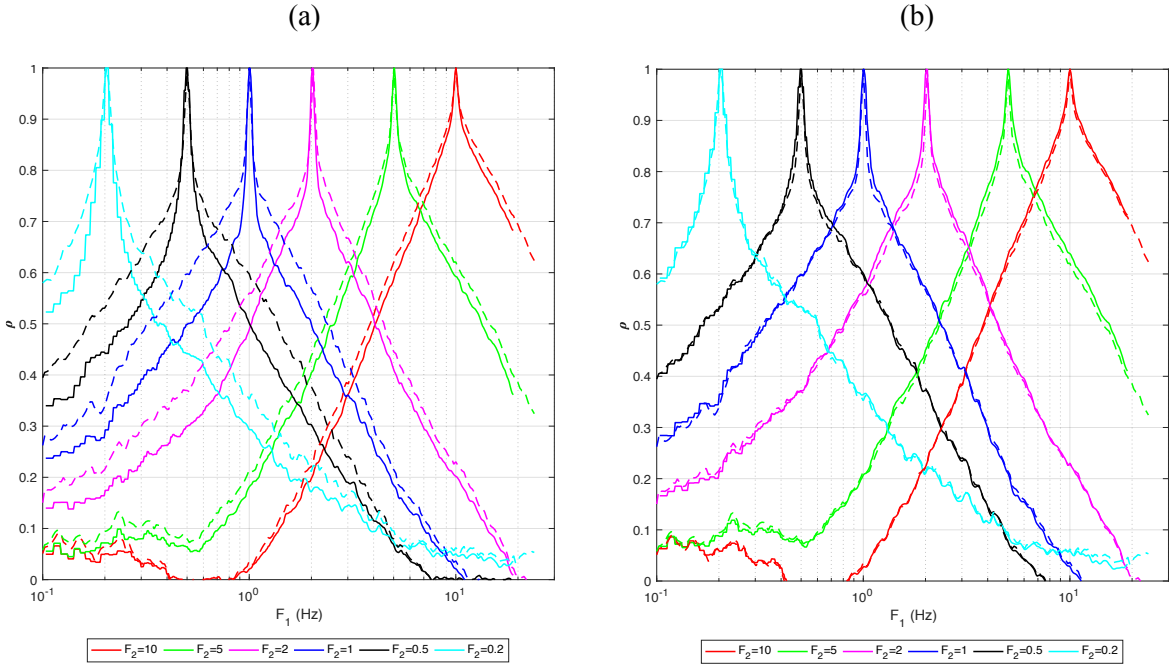

Figure 1. The inter-frequency correlation coefficients of epsilon at reference frequencies 0.2 Hz, 0.5 Hz, 1 Hz, 2 Hz, 5 Hz and 10 Hz from the empirical correlation coefficients (dashed lines) and the SDSU SCEC BBP Module after applying our method. (a) Using independent random variables at two horizontal components (solid lines), and (b) using correlated random variables (with correlation coefficient equals 0.7) at two horizontal components (solid lines) for the Loma Prieta event.

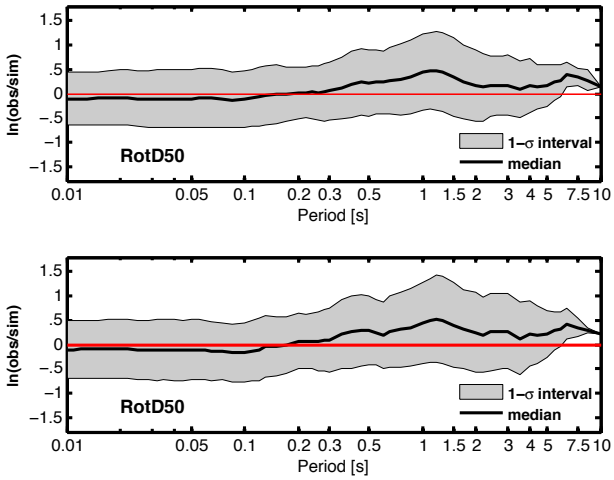

Figure 2. The natural log of the misfit between median RotD50 PSA for observations and predictions using 50 source realizations for the original (uncorrelated) (top) and (bottom) correlated SDSU synthetics for the Loma Prieta event.

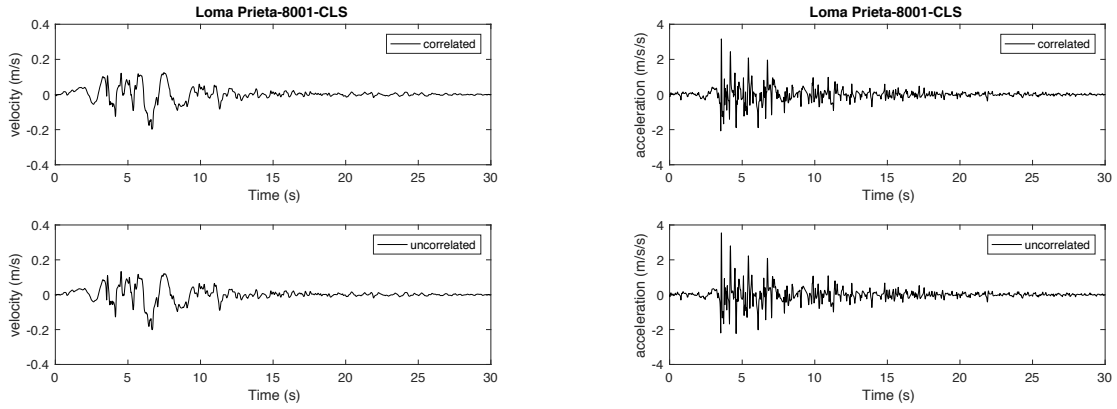

Figure 3. Examples of the north-south component of velocities (left) and accelerations (right) at station 8001-CLS for Loma Prieta event after (top) and before (bottom) implementing the inter-frequency correlations.

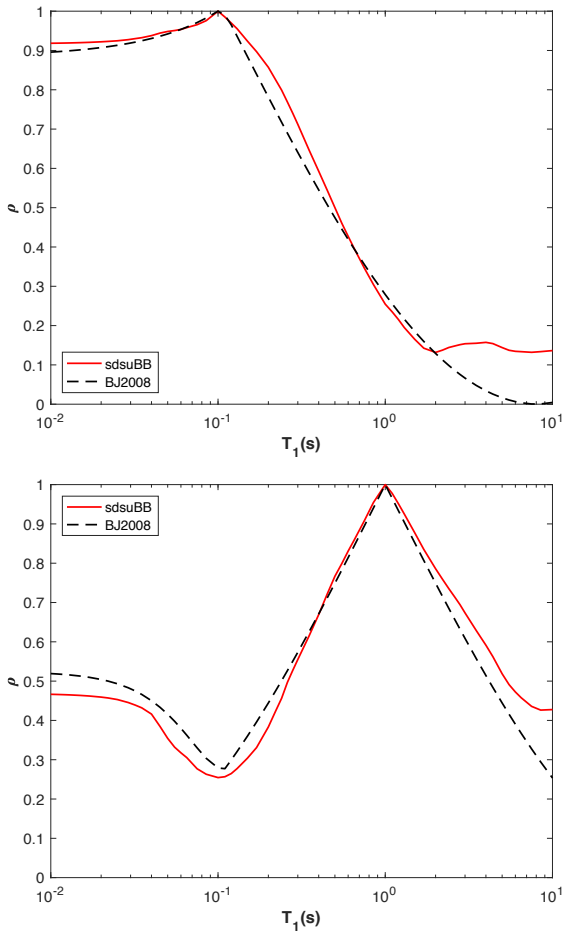

Figure 4. Comparison of the inter-frequency spectral acceleration correlation coefficients of epsilon at reference periods 0.1 s (top) and 1 s (bottom) from the Baker and Jayaram (2008) model (dashed black lines) and the SDSU SCEC BBP Module after applying our method (solid red lines) for the Loma Prieta event with 50 realizations.

References

Abrahamson, N. A., Silva, W. J., and Kamai, R. (2014). Summary of the ASK14 ground motion relation for active crustal regions. *Earthquake Spectra, 30*(3), 1025-1055.

Akkar, S., Sandıkkaya, M. A., and Ay, B. Ö. (2014). Compatible ground-motion prediction equations for damping scaling factors and vertical-to-horizontal spectral amplitude ratios for the broader Europe region. *Bulletin of earthquake engineering, 12*(1), 517-547.

Al Atik, L., Abrahamson, N., Bommer, J. J., Scherbaum, F., Cotton, F., and Kuehn, N. (2010). The variability of ground-motion prediction models and its components. *Seismological Research Letters, 81*(5), 794-801.

Atkinson, G. M., and Assatourians, K. (2015). Implementation and validation of EXSIM (a stochastic finite‐fault ground‐motion simulation algorithm) on the SCEC broadband platform. *Seismological Research Letters, 86*(1), 48-60.

Azarbakht, A., Mousavi, M., Nourizadeh, M., and Shahri, M. (2014). Dependence of correlations between spectral accelerations at multiple periods on magnitude and distance. *Engineering and Structural Dynamics, 43*(8), 1193-1204.

Baker, J. W., and Bradley, B. A. (2017). Intensity measure correlations observed in the NGA-West2 database, and dependence of correlations on rupture and site parameters. *Earthquake Spectra, 33*(1), 145-156.

Baker, J. W., and Cornell, C. A. (2006). Spectral shape, epsilon and record selection. *Earthquake Engineering and Structural Dynamics, 35*(9), 1077-1095.

Baker, J. W., and Jayaram, N. (2008). Correlation of spectral acceleration values from NGA ground motion models. *Earthquake Spectra, 24*(1), 299-317.

Bayless, J. R., Somerville, P. G., Skarlatoudis, A., Silva, F., and Abrahamson, N. A. (2016). Inter-Period Correlations of SCEC Broadband Platform Fourier Amplitudes and Response Spectra. *Poster Presentation at 2016 SCEC Annual Meeting.* Palm Springs, California.

Bayless, J., and Abrahamson, N. A. (2018a). An empirical model for Fourier amplitude spectra using the NGA-West2 database. *in preparation*.

Bayless, J., and Abrahamson, N. A. (2018b). Evaluation of the Interperiod Correlation of Ground‐Motion Simulations. *Bulletin of the Seismological Society of America, 108*(6), 3413-3430.

Bommer, J. J., and Crowley, H. (2006). The influence of ground-motion variability in earthquake loss modelling. *Bulletin of Earthquake Engineering, 4*(3), 231-248.

Boore, D. M. (2003). Simulation of ground motion using the stochastic method. *Pure and applied geophysics, 160*(3-4), 635-676.

Boore, D. M., Gibbs, J. F., Joyner, W. B., Tinsley, J. C., and Ponti, D. J. (2003). Estimated ground motion from the 1994 Northridge, California, earthquake at the site of the Interstate 10 and La Cienega Boulevard bridge collapse, West Los Angeles, California. *Bulletin of the Seismological Society of America, 93*(6), 2737-2751.

Burks, L. S., and Baker, J. W. (2014). Validation of ground‐motion simulations through simple proxies for the response of engineered systems. *Bulletin of the Seismological Society of America, 104*(4), 1930-1946.

Cimellaro, G. P. (2013). Correlation in spectral accelerations for earthquakes in Europe. *Earthquake Engineering and Structural Dynamics, 42*(4), 623-633.

Crempien, J. G., and Archuleta, R. J. (2015). UCSB method for simulation of broadband ground motion from kinematic earthquake sources. *Seismological Research Letters, 86*(1), 61-67.

Esposito, S., and Iervolino, I. (2011). PGA and PGV spatial correlation models based on European multievent datasets. *Bulletin of the Seismological Society of America, 101*(5), 2532-2541.

Fisher, R. A. (1958). *Statistical Methods for Research Workers* (Vol. 13th Ed). Edinburgh, London, United Kingdom: Hafner.

Goda, K., and Atkinson, G. M. (2009). Probabilistic characterization of spatially correlated response spectra for earthquakes in Japan. *Bulletin of the Seismological Society of America, 99*(5), 3003-3020.

Goda, K., and Hong, H.-P. (2008). Spatial correlation of peak ground motions and response spectra. *Bulletin of the Seismological Society of America, 98*(1), 354-365.

Goulet, C., Abrahamson, N., Somerville, P., and Wooddell, K. (2015). The SCEC Broadband Platform validation exercise for pseudo‐spectral acceleration: Methodology for code validation in the context of seismic hazard analyses. *Seismological Research Letters, 86*(1).

Graves, R., and Pitarka, A. (2015). Refinements to the Graves and Pitarka (2010) broadband ground‐motion simulation method. *Seismological Research Letters, 86*(1), 75-80.

Heresi, P., and Miranda, E. (2019). Uncertainty in intraevent spatial correlation of elastic pseudo-acceleration spectral ordinates. *Bulletin of Earthquake Engineering, 17*(3), 1099-1115.

Hole, J. A. (1992). Nonlinear high‐resolution three‐dimensional seismic travel time tomography. *Journal of Geophysical Research: Solid Earth, 97*(B5), 6553-6562.

Hong, H. P. (2000). Distribution of structural collapses and optimum reliability for infrequent environmental loads. *Structural safety, 22*(4), 297-311.

Jayaram, N., and Baker, J. W. (2009). Correlation model for spatially distributed ground‐motion intensities. *Earthquake Engineering and Structural Dynamics, 38*(15), 1687-1708.

Kawakami, H., and Mogi, H. (2003). Analyzing spatial intraevent variability of peak ground accelerations as a function of separation distance. *Bulletin of the Seismological Society of America, 93*(3), 1079-1090.

Konno, K., and Ohmachi, T. (1998). Ground-motion characteristics estimated from spectral ratio between horizontal and vertical components of microtremor. *Bulletin of the Seismological Society of America, 88*(1), 228-241.

Kottke, A., Abrahamson, N. A., Boore, D. M., Bozorgnia, Y., Goulet, C., Hollenback, J., . . . Wang, X. (2018). Selection of Random Vibration Procedures for the NGA-East Project. *PEER report*.

Kutner, M. H., Nachtsheim, C., and Neter, J. (2004). *Applied linear regression models, 4th Ed.* New York: McGraw-Hill/Irwin.

Loth, C., and Baker, J. W. (2013). A spatial cross‐correlation model of spectral accelerations at multiple periods. *Earthquake Engineering and Structural Dynamics, 42*(3), 397-417.

Mai, P. M., Imperatori, W., and Olsen, K. B. (2010). Hybrid broadband ground-motion simulations: Combining long-period deterministic synthetics with high-frequency multiple S-to-S backscattering. *Bulletin of the Seismological Society of America, 100*(5A), 2124-2142.

Markhvida, M., Ceferino, L., and Baker, J. W. (2018). Modeling spatially correlated spectral accelerations at multiple periods using principal component analysis and geostatistics. *Earthquake Engineering and Structural Dynamics, 47*(5), 1107-1123.

Mena, B., Mai, P. M., Olsen, K. B., Purvance, M. D., and Brune, J. N. (2010). Hybrid broadband ground-motion simulation using scattering Green's functions: Application to large-magnitude events. *Bulletin of the Seismological Society of America, 100*(5A), 2143-2162.

Olsen, K. B., and Takedatsu, R. (2015). The SDSU broadband ground‐motion generation module BBtoolbox version 1.5. *Seismological Research Letters, 86*(1), 81-88.

Seber, G. A., and Lee, A. J. (2012). *Linear regression analysis.* John Wiley and Sons.

Seifried, A. E., and Baker, J. W. (2016). Spectral variability and its relationship to structural response estimated from scaled and spectrum-matched ground motions. *Earthquake Spectra, 32*(4), 2191-2205.

Seydel, R. (2012). Generating Random Numbers with Specified Distributions. In *Tools for Computational Finance, Universitext.* London, United Kingdom: Springer.

Sokolov, V., and Wenzel, F. (2013). Further analysis of the influence of site conditions and earthquake magnitude on ground-motion within-earthquake correlation: analysis of PGA and PGV data from the K-NET and the KiK-net (Japan) networks. *Bulletin of Earthquake Engineering, 11*(6), 1909-1926.

Sokolov, V., Wenzel, F., Wen, K.-L., and Jean, W.-Y. (2012). On the influence of site conditions and earthquake magnitude on ground-motion within-earthquake correlation: analysis of PGA data from TSMIP (Taiwan) network. *Bulletin of Earthquake Engineering, 10*(5), 1401-1429.

Stafford, P. J. (2017). Stafford, P.J., 2017. Interfrequency Correlations among Fourier Spectral Ordinates and Implications for Stochastic Ground‐Motion SimulationInterfrequency Correlations among Fourier Spectral Ordinates and Implications. *Bulletin of the Seismological Society of America, 107*(6), 2774-2791.

Stafford, P. J., and Bommer, J. J. (2010). Theoretical consistency of common record selection strategies in performance-based earthquake engineering. *In Advances in Performance-Based Earthquake Engineering*, 49-58.

Wang, M., and Takada, T. (2005). Macrospatial correlation model of seismic ground motions. *Earthquake spectra, 21*(4), 1137-1156.

Weatherill, G. A., Silva, V., Crowley, H., and Bazzurro, P. (2015). Exploring the impact of spatial correlations and uncertainties for portfolio analysis in probabilistic seismic loss estimation. *Bulletin of Earthquake Engineering, 13*(4), 957-981.

Wesson, R. L., and Perkins, D. M. (2001). Spatial correlation of probabilistic earthquake ground motion and loss. *Bulletin of the Seismological Society of America, 91*(6), 1498-1515.

Wharf, C. A. (2016). Discrete multivariate representation of Fourier spectral ordinates, M.Sc. Thesis.

Zeng, Y., Aki, K., and Teng, T.‐L. (1993). Mapping of the high‐frequency source radiation for the Loma Prieta earthquake, California. *Journal of Geophysical Research: Solid Earth, 98*(B7), 11981-11993.

Zeng, Y., Su, F., and Aki, K. (1991). Scattering wave energy propagation in a random isotropic scattering medium: 1. Theory. *Journal of Geophysical Research: Solid Earth, 96*(B1), 607-619.